Effects of compaction on soil undrained shear strength deteriorating during undrained cyclic loading and controlling seismic stability of embankment

Antoine Duttine[1,*], *Fumio* Tatsuoka[2], and *Kazuhiro* Ueno[3]

[1]Integrated Geotechnology Institute Ltd, Engineering and Numerical Analysis Department, Tokyo, Japan
[2]Tokyo University of Science, Civil Engineering Department, Chiba, Japan
[3]Shimane University, Department of Environmental Systems, Shimane, Japan

Abstract. Effects of compaction on the undrained shear strength of saturated earth-fill dam materials are presented. Poorly and well compacted saturated soils may exhibit undrained shear strengths, respectively, significantly lower and higher than corresponding drained shear strength and this trend is amplified as the undrained strength deteriorates by preceding undrained cyclic loading. These features are implemented in a new simplified seismic analysis to evaluate residual deformation of earth-fill dams. The analysis consists of: 1) a modified Newmark sliding block analysis; and 2) a pseudo-static non-linear FEM analysis, both formulated in a unified framework based on the cumulative damage concept, total stress earthquake response analysis and a direct total stress modelling of undrained monotonic and cyclic stress-strain behaviours obtained by triaxial tests. The analysis simulates very well the collapse of an earth-fill dam by the 2011 Off the Pacific Coast of Tohoku Earthquake, Japan, and indicates a substantially higher seismic stability under the same conditions of the newly restored dam completed in 2017. Paramount effects of soil compaction on the seismic stability of earth-filled dam are demonstrated.

1 Introduction

Around 2,000 of the 12,500 irrigation earth-fill dams in Iwate, Miyagi and Fukushima Prefectures in Japan were seriously damaged during the 2011 Off the Pacific Coast Tohoku Earthquake (magnitude M=9.0) [1]. The main and auxiliary dams of Fujinuma Reservoir, located on the branch of upper Sunoko River in Fukushima Prefecture (Fig. 1), totally collapsed by the earthquake. The main dam breached resulting in a flood (indicated by a red arrow in Fig. 1a) that caused seven deaths and one missing [2].

As detailed later, the primary cause of the collapse was generally poor compaction of the dam body. In particular with the old main dam, the compaction of the sandy top fill was very poor, which resulted in a very low initial undrained shear strength that largely deteriorated by undrained cyclic loading (UCL) during a particularly long earthquake motion [2].

To reach these conclusions, dry densities of the fills remaining after the collapse were evaluated and laboratory compaction tests were performed on samples retrieved from the field. A series of undrained triaxial compression (TC) tests were also performed on specimens compacted to the field densities and those compacted looser or denser. Undrained shear strengths before and after undrained cyclic loading (UCL) histories causing different strains were also evaluated [4, 5].

It is difficult to predict such collapse when based on the conventional design procedure for irrigation earth-fill

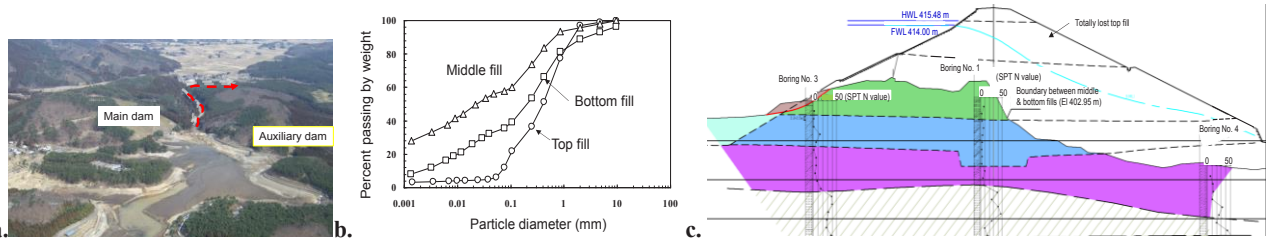

Fig. 1. a) Aerial picture of Fujinuma dams taken immediately after collapse; b) grading properties of fill materials; and c) central cross-section of main dam (height=18.5m) before and after collapse (after [2], [3]).

* Corresponding author: antoine@igi.co.jp

dams in Japan, which is based on an allowable lower bound of the global safety factor by pseudo-static limit equilibrium method using the drained shear strength of soil. On the other hand, non-linear FEM effective stress analyses remain too sophisticated and too costly in engineering practice due to a number of highly complicated issues including: a) build-up/dissipation of excessive pore water pressure both globally and locally around and inside shear bands having a thickness controlled by particle size; b) effects of dilatancy characteristics under cyclic loading; c) proper undrained stress-strain modelling of well compacted soil. In view of the above, a pair of new simplified analysis methods was developed incorporating TC test results formulated in a unified and straightforward framework based on the cumulative damage concept combined with total stress earthquake response analysis [4, 5]. By this method, the collapse of the old main dam was simulated very well, as shown below.

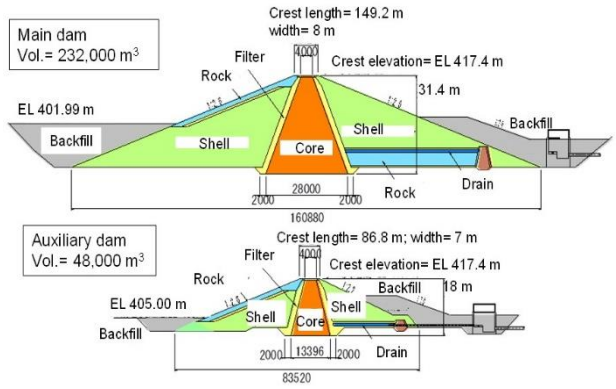

Fig. 2. Central cross-sections of newly restored Fujinuma dams (height= 31.4 m and 18m).

The collapsed dams were restored to new modern earth-fill dams (Fig. 2) to be much more stable than the old ones. They were designed based on the seismic stability analysis explained in details below. The core and shelter were compacted following a new soil compaction procedure, which is presented in the companion paper [6]. Restoration was completed in January 2017. A set of laboratory stress-strain tests was then performed on the fill materials used to construct the dams precisely at field compacted states. The results of the seismic stability analysis of the new main dam evaluated by the same analysis method and under otherwise the same conditions as the analysis of the collapsed old main dam are reported below.

2 Laboratory stress-strain tests

2.1 Old Fujinuma dam

A series of undrained TC tests were performed on specimens reconstituted using samples retrieved from the remaining part of the top fill (F_c=12%, NP, U_c=7.4), middle fill (F_c=57.8%, I_p=31.6) and bottom fill (F_c=35.5%, NP, U_c=156) of the old main dam (Fig. 1). Specimens were compacted closely to the measured field dry densities: (top fill) ρ_d (g/cm^3)= 1.39 & $[D_c]_{1Ec}$ (%)= 87.9; (middle fill) ρ_d= 0.95 & $[D_c]_{1Ec}$=84.5; and (bottom fill) ρ_d= 1.31 & $[D_c]_{1Ec}$= 90.1 at respective optimum water contents by Standard Proctor (1Ec). They were made saturated using a back pressure of 200 kPa and anisotropically consolidated at a ratio of effective axial to radial stresses of 2.0 to respective estimated average field stress states. UCL was performed by using uniform symmetric sinusoidal waves at a frequency of 0.1 Hz.

Typical test results are presented in Figs. 3 & 4. The top fill specimens exhibit a strong trend of contractive behaviour at the initial stage of undrained loading, which resulted in relatively low initial undrained shear strengths (Figs. 3a & b). In comparison, the middle fill specimens exhibit less contractive behaviour, showing a relatively denser compacted state (Figs. 4a & b). Besides, with both fill materials, the ultimate undrained shear strength by undrained monotonic loading (UML) decreases with an increase in the maximum axial strain that has developed by precedent UCL.

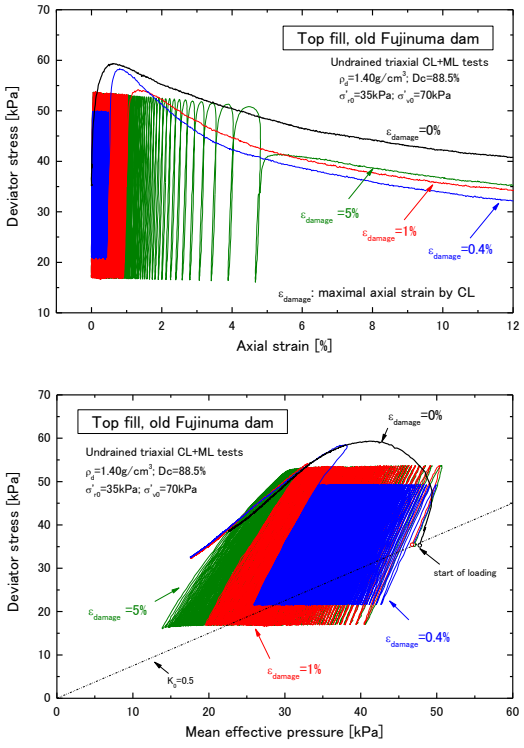

Fig. 3. Typical undrained stress-strain behaviours and effective stress paths before and after applications of different UCL histories (old dam, top fill) [3]

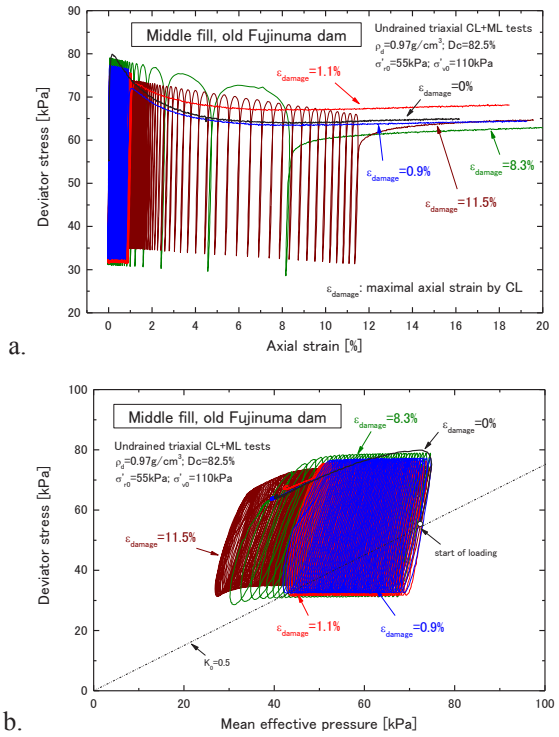

Fig. 4. Typical undrained stress-strain behaviours and effective stress paths before and after applications of different UCL histories of middle fill [3]

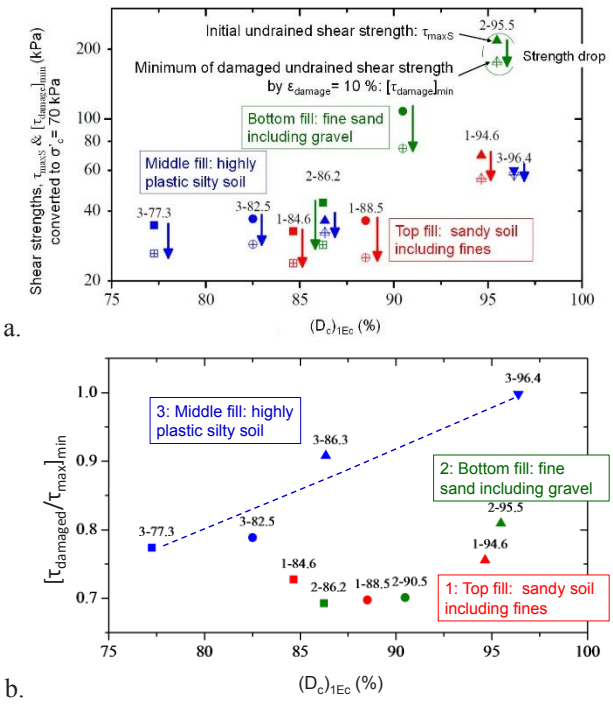

Fig. 5. Undrained shear strengths of specimens compacted to different dry densities: a) initial and damaged strengths converted to σ'$_c$=70kPa; b) ratio of the damaged strength to the initial strength in a function of $[D_c]_{1Ec}$ [3]

Fig. 5a shows the initial and deteriorated undrained shear strengths obtained from this and other similar series of undrained TC tests on specimens compacted to different dry densities, which are plotted in logarithmic scale against $[D_c]_{1Ec}$. These undrained strengths have been converted to those at an effective consolidation pressure σ'$_c$ equal to 70 kPa by assuming that the undrained strength is proportional to σ'$_c$. The initial undrained strength becomes much higher when compacted sufficiently denser than the respective field compacted states: i.e., $[D_c]_{1Ec}$= 87.9 % (top fill); 84.5 % (middle fill); and 90.1 % (bottom fill). The deteriorated strengths are those observed until the axial strain became about 10 % in UML performed after applications of various UCL histories. As seen from Fig. 5b, for a same $[D_c]_{1Ec}$, the decreasing rate of undrained strength is smaller with the middle fill material (having the largest fines content) than with the top fill material (non-plastic having the least fines contents) and the bottom fill material with an intermediate grading. Besides, with the respective fill materials, with an increase in $[D_c]_{1Ec}$, the initial undrained strength increases while the decreasing rate of undrained strength decreases. As a result, the deteriorated strength increases significantly with $[D_c]_{1Ec}$, particularly with the bottom fill material (Fig. 5a).

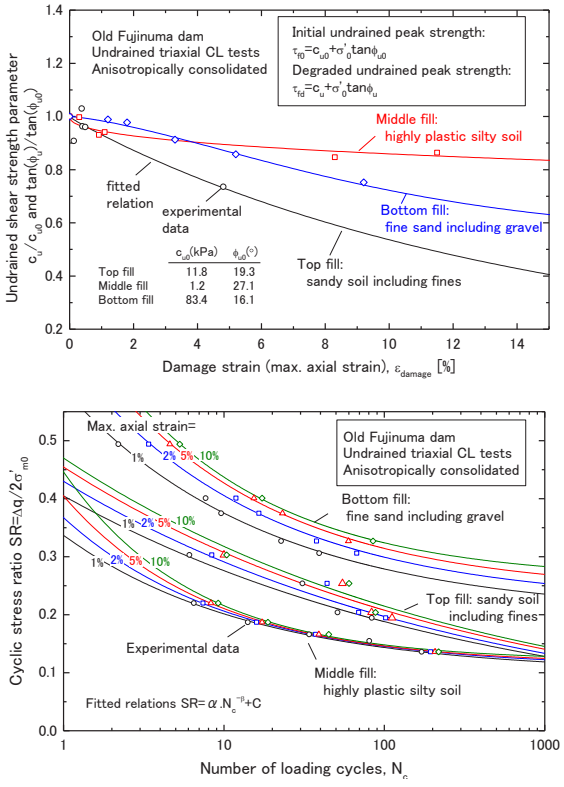

Fig. 6. a) Ratio of deteriorated undrained shear strength to initial value plotted against damage strain; and b) fatigue curves obtained by undrained CL triaxial tests (old dam).

For the seismic stability analysis reported hereafter, the undrained shear strength was modelled by the so-called total stress method. That is, the initial undrained shear strength is represented by $(\tau_{fu})_0$= c_{u0}+σ'$_{n0}$.tanϕ$_{u0}$ and the deteriorated undrained strength after UCL by τ_{fu}= c_u+ σ'$_{n0}$.tanϕ$_u$, where σ'$_{n0}$ is the initial effective normal stress activated at respective places along the failure plane. It is assumed that, with an increase in the damage strain during precedent UCL, the linear strength envelop rotates about a fixed origin along the σ-axis in such that the strength

ratio $\tau_{fu}/(\tau_{fu})_0$ is always kept equal to $c_u/c_{u0}= \tan\phi_u/\tan\phi_{u0}$. Fig. 6a shows the measured values of this ratio plotted against the respective damage strains. It may be seen that the deterioration rate is smallest with the middle fill and largest with the top fill showing that this rate increases with a decrease in the fines content. These relations were fitted by Eq. 1 to be used in the stability analysis:

$$y=A_1.exp[-(\varepsilon_{damage}/t_1)^{d1}]+A_2.exp[-(\varepsilon_{damage}/t_2)^{d2}] \quad (1)$$

where A_1, t_1, d_1, A_2=1-A_1, t_2 and d_2 are constants.

Fig. 6b shows the relationships between the single amplitude cyclic shear stress ratio SR and the number of loading cycles N_c necessary to develop different maximum axial strains (i.e. fatigue curves). The SR value that is defined for a same strain and N_c is largest with the bottom fill (compacted relatively dense) and quite low with the top and middle fills (compacted loose).

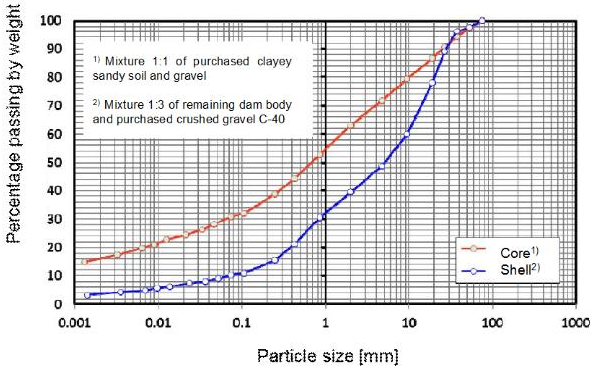

Fig. 7. Grading curves representative of restored dam

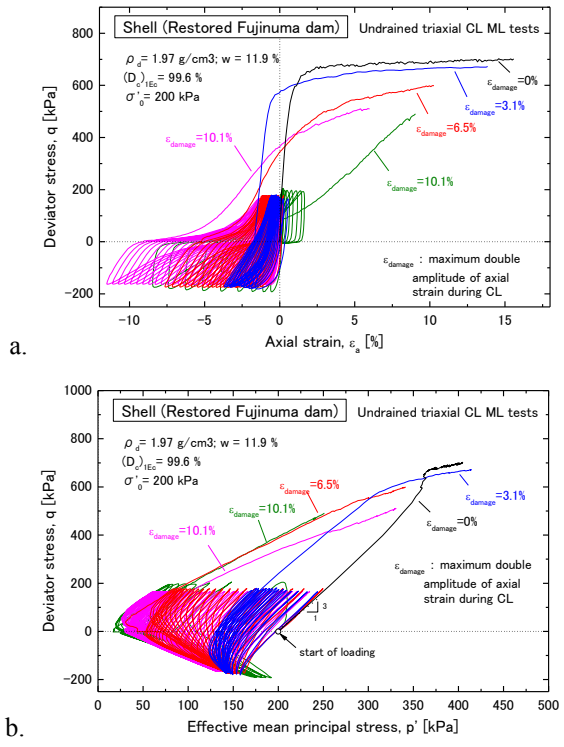

Fig. 8. Undrained stress-strain curves and effective stress paths before and after various UCL histories (shell of new main dam)

2.2 Restored Fujinuma dam

A similar series of undrained TC tests were performed on reconstituted specimens of the fill materials used to construct the shell and core of the restored main dam (Figs. 2 & 7). Specimens compacted to the estimated average field compacted states (i.e., $[D_c]_{1Ec}$= 99.6 % at S_r= $(S_r)_{opt}$= 84.1 % for shell and $[D_c]_{1Ec}$= 99.2 % at S_r= $(S_r)_{opt}$= 89.2 % for core; see Fig. 10 of Tatsuoka & Miura 2019) were isotropically consolidated to the respective average field stress levels and subjected to UCL at a frequency of 0.1 Hz. Fig. 8 shows typical test results. Fig. 9a shows the ratios of the undrained strength that has deteriorated by various UCL histories to the initial value of core and shell materials, plotted against the maximum axial strain that developed during the respective UCL. Fig. 9b shows the fatigue curves obtained from the UCL phases. Compared to the fill materials of the old dam (Figs. 3, 4 & 6), the shell and core materials of the new dam exhibit: a) much higher initial undrained strengths (Fig. 8); b) much lower deterioration rates for a given damage strain (e.g., 10 %) (Fig. 9a); and c) noticeably higher SR values for the same strain and N_c (Fig. 9b). These trends are due to substantially higher $[D_c]_{1Ec}$ values achieved in the restored dams. These and other stress-strain properties were implemented in the seismic stability analyses described below.

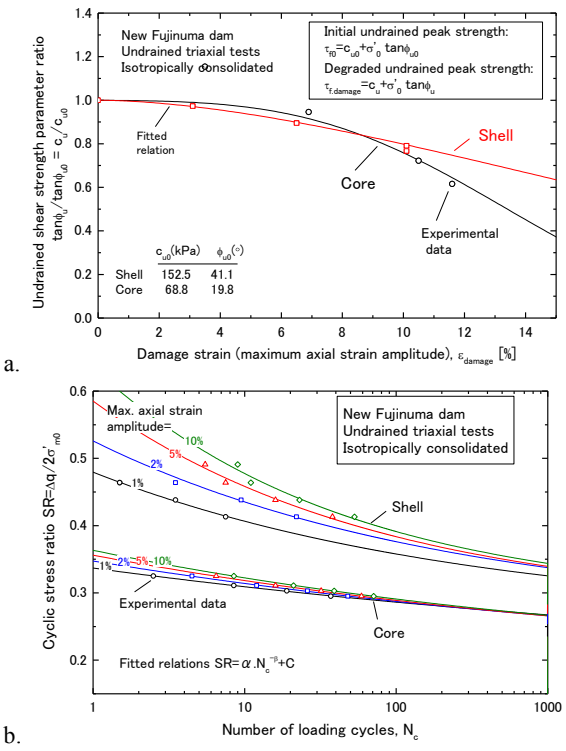

Fig. 9. a) Ratio of deteriorated undrained strength to initial value; and b) fatigue curves obtained by UCL (new main dam).

3 Simplified seismic stability analysis

The following numerical analyses were performed to evaluate the seismic-induced residual displacement and deformation of the old and new main dams [4, 5]:

1) *Plane strain 2D FEM equivalent-linear dynamic response analysis in the frequency domain to obtain the time histories of response acceleration and mobilized stresses*: It was confirmed that results are very similar to those obtained by a non-linear seismic response analysis in the time domain under otherwise the same conditions. Possible effects of degradation of non-linear stress-strain properties in the course of UCL were ignored. This method somehow over-estimates mobilized cyclic stresses therefore is on the safe side in usual design cases, where the natural frequency of fill dam decreases by the degradation of stress-strain properties from the initial value that is lower than predominant frequencies of major earthquakes usually considered in design.

2) *Modified Newmark sliding block analysis taking into account the degradation of undrained shear strength by irregular UCL during seismic loading*: For given cyclic undrained stress-strain properties (as described in Figs. 6b & 9b), the maximum strain (i.e., the damage strain) that has taken place by a given moment during a given time history of cyclic shear stress evaluated by analysis 1 above is obtained by the cumulative damage concept [7]. The instantaneous undrained shear strength is obtained by reducing the initial value by the degraded-to-initial strength ratio obtained by substituting the current damage strain into relevant relations, such as presented in Figs. 6a and 9a. Time histories of slip displacement for many relevant trial slip circles are obtained using the time histories of undrained shear strength of all saturated FEM elements. The critical slip plane is determined as the one that gives the maximum sliding displacement.

3) *Plane strain 2D pseudo-static non-linear FEM analysis to evaluate the residual deformation by self-weight and seismic inertial forces obtained by analysis 1*: The residual deformation at the end of seismic loading is assumed to be equal to the maximum deformation that has taken place by the end of seismic loading. The deformation excluding the one by slip failure at a given moment is computed by this FEM analysis, using instantaneous undrained pre-peak stress-strain relations of saturated FEM elements that have deteriorated as the damage strain increases, following a similar procedure as 2). Seismic inertia forces at this given moment are computed from node accelerations obtained in 1).

Assuming that the sliding body is rigid once the sliding starts, the total ultimate residual deformation is then obtained by combining the ultimate rotational rigid block displacement of the modified Newmark analysis with the ultimate residual displacement obtained by the pseudo-static non-linear FEM analysis.

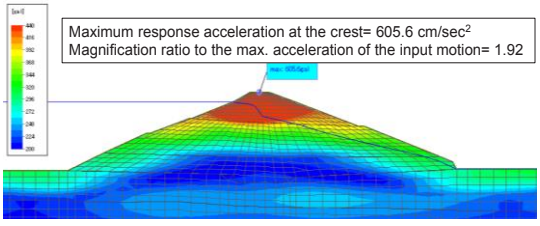

Fig. 10. Contours of maximum response acceleration obtained by equivalent-linear dynamic response analysis (old main dam).

Fig. 10 shows the results of seismic response analysis of the old main dam. For this analysis, the values of initial shear modulus G_0 were estimated by PS loggings performed in the remaining parts of the old main dam (Fig. 1). The non-linear G_{eq}/G_0 & h - γ properties were estimated from data of similar soil types reported in the literature (Public Work Research Institute, Japanese Government). For the new main dam, those properties were obtained by performing relevant laboratory stress-strain tests. The same input bedrock motion, derived from the time history of horizontal ground acceleration recorded during the 2011 Great East Japan Earthquake at Naganuma (FKSH08), 3 km NW from Fujinuma dam, was used in the analysis of both old and new dams.

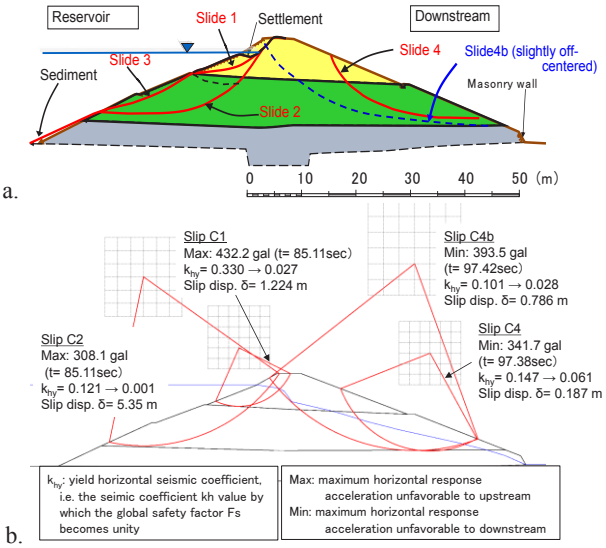

Fig. 11. a) Slip planes inferred by field investigations (after [2]); and b) critical slip circles obtained by modified Newmark analysis (old main dam)

Fig. 11b shows the critical slip circles obtained by the modified Newmark analysis, which are remarkably consistent with the actual ones inferred by field investigation after the collapse (Fig. 11a). As indicated in Fig. 11b, the yield horizontal seismic coefficient, k_{hy}, along these critical slip circles becomes very low by the end of seismic loading, which results in significant sliding displacements. Fig. 12 shows the ultimate residual deformation obtained by combining those by the two analysis methods when slips C1, C2 and C4b take place separately. Large residual deformation at crest obtained by summing up these results is consistent with the over-topping flow that actually took place and resulted in the breaching of the old main dam.

Fig. 13 shows the ultimate residual deformation of the restored main dam under the same conditions and obtained by the same analysis method. No rigid slip displacement takes place due to high initial yield seismic coefficients along the critical slip circles, k_{hy}= 1.068 (upstream slope) and 0.696 (downstream slope), which only slightly decreases by seismic loading. Besides, the

residual deformation by pseudo-static FEM analysis remains very small (i.e., a crest settlement equal to 7 cm).

Fig. 14 shows the average drained and undrained shear strengths mobilized along slip C1 in the old main dam and a slip at a similar location in the new main dam plotted against the degree of compaction, $[D_c]_{1Ec}$, used in the analysis. The compacted states in the old and new main dams are indicated by two short vertical arrows. During the earthquake, the undrained shear strength decreases by UCL, while the drained shear strength decreases by a decrease in the normal stress along the slip circle by seismic inertia.

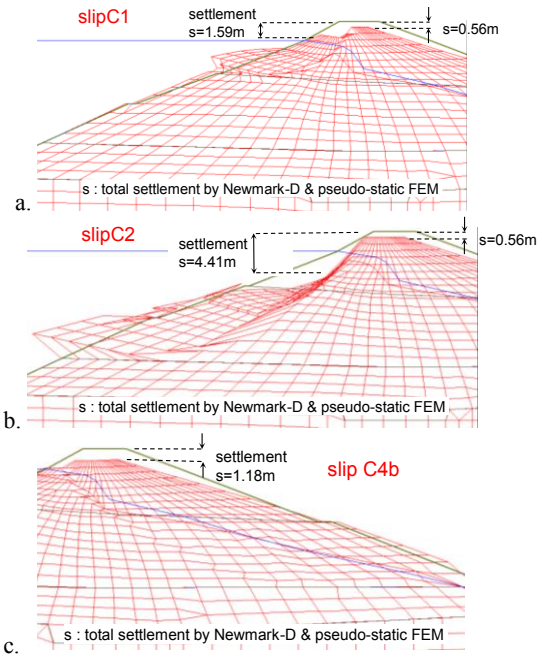

Fig. 12. Combined residual deformation for each slip by Newmark and pseudo-static FEM analyses (old main dam)

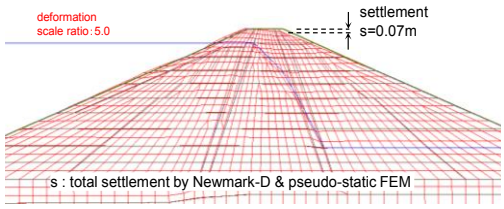

Fig. 13. Combined residual deformation by Newmark and pseudo-static FEM analyses (new main dam)

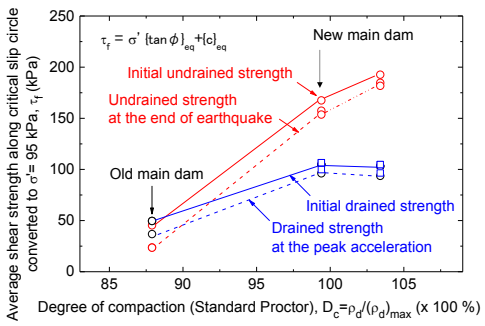

Fig. 14. Initial and deteriorated undrained shear strengths compared with drained strength as a function of $[D_c]_{1Ec}$.

Significant effects of compaction may be seen in Fig.14. That is, the initial undrained strengths of the poorly compacted materials of the old main dam and the well compacted materials of the new main dam are respectively noticeably lower and significantly higher than their corresponding initial drained strength and this trend is amplified after having been deteriorated by UCL.

4 Conclusions

Series of undrained monotonic triaxial compression tests were performed before and after applying undrained cyclic loading histories developing different strains on saturated poorly compacted specimens of the fill materials retrieved from of a 18.5 m-high Fujinuma main dam that collapsed by the 2011 Off the Pacific Coast of Tohoku Earthquake. Similar tests were performed on much better compacted shell and core materials of the restored main dam. "Rigid slip analysis by the modified Newmark method" combined with "residual deformation analysis by a pseudo-static non-linear FEM" using these laboratory test data modelled in a single framework simulates very well the collapse of the old main dam and indicates a high seismic stability of the new dams showing paramount importance of good soil compaction for a high seismic stability of fill dam.

The authors would like to express their sincere gratitude to Prof. Tanaka, T., Prof. Mohri, Y. and Fukushima Prefecture for their help in performing this study.

References

1. Japan Rural Development Bureau (JRDB), On the revision of earth fill dam design codes, *Japan Ministry of Agriculture, Forestry and Fisheries*, Doc. No. 4, (in Japanese) (2012)
2. T. Tanaka, F. Tatsuoka, Y. Mohri, Y., Earthquake-induced failure of Fujinuma Dam, *Proc. Int. Symp. On Dams for a Changing World*, 24th Congress ICOLD, Kyoto (2012)
3. K. Ueno, Y. Mohri, T. Tanaka, F. Tatsuoka, Effects of compaction degree on the strength reduction rate by cyclic undrained loading of saturated soil, *Proc. 49th Japan National Conference on Geotechnical Eng., Kitakyushu,* 1395-1396 (in Japanese) (2014)
4. F. Tatsuoka, T. Tanaka, K. Ueno, A. Duttine, Y. Mohri, Soil properties and seismic stability of old and new Fujinuma dams, *Proc. Int. Symp. on Qualification of dynamic analyses of dams and their equipment, Saint-Malo, France* (eds. Fry, J.-J. & Matsumoto, N.), 119-170 (2018)
5. A. Duttine, F. Tatsuoka, T. Shinbo, Y. Mohri, A new simplified seismic stability analysis taking into account degradation of soil undrained stress – strain properties and effects of compaction, *Proc. Int. Sym. on Qualification of dynamic analyses of dams and their equipment, Saint-Malo, France* (eds. Fry, J.-J. & Matsumoto, N.), 215-234 (2018)
6. F. Tatsuoka, F.T. Miura, Compacted states and

physical properties of soil controlled by the degree of saturation during compaction, *Proc. 7th Int. Symp. on Deformation Characteristics of Geo-materials, IS-Glasgow* (2019)

7. N.C. Donovan, A stochastic approach to the liquefaction problem, *Proc. Int. Conf. On Application of Statistics and Probability to Soil and Structural Eng.*, HongKong, 513-535 (1971)